Chapter 10
Thermoelectric Properties of $CoSb_3$ Based Skutterudites Filled by Group 13 Elements

Ken Kurosaki, Adul Harnwunggmoung, and Shinsuke Yamanaka

Abstract Thermoelectric (TE) generators can directly generate electrical power from waste heat, and thus could be an important part of the solution to future power supply and sustainable energy management. The main obstacle to the widespread use of TEs in diverse industries, e.g., for exhaust heat recovery in automobiles, is the low efficiency of materials in converting heat to electricity. The conversion efficiency of TE materials is quantified by the dimensionless figure of merit, ZT, and the way to enhance ZT is to decrease the lattice thermal conductivity (κ_{lat}) of the material, while maintaining a high electrical conductivity, i.e., to create a situation in which phonons are scattered but electrons are unaffected. Various concepts have been used in the search for this situation, e.g., the use of rattling of atoms weakly bonded in crystals and nanostructuring of materials. Here we report TE properties of skutterudites filled by group 13 elements, i.e., Ga, In, and Tl. Our group has examined the high-temperature TE properties of various skutterudites filed by group 13 elements, viz., Ga-filled $CoSb_3$, Tl-filled $CoSb_3$, and In/Tl double-filled $CoSb_3$. All systems exhibit relatively high TE figure of merit, especially, $Tl_{0.1}In_xCo_4Sb_{12}$ achieves a dramatic reduction of κ_{lat}, resulting in the $ZT = 1.20$ at 700 K—very high for a bulk material. We have demonstrated that the reduction of κ_{lat} in $Tl_{0.1}In_xCo_4Sb_{12}$ is due to the effective phonon scattering both by rattling of two atoms: Tl and In and by naturally formed nano-sized In_2O_3 particles (<50 nm).

K. Kurosaki (✉) • S. Yamanaka
Division of Sustainable Energy and Environmental Engineering, Graduate School of Engineering, Osaka University, 2-1 Yamadaoka, Suita, Osaka 565-0871, Japan
e-mail: kurosaki@see.eng.osaka-u.ac.jp; yamanaka@see.eng.osaka-u.ac.jp

A. Harnwunggmoung
Thermoelectric and Nanotechnology Research Center, Faculty of Science and Technology, Rajamangala University of Technology Suvarnabhumi, Huntra, Phranakhon Si Ayutthaya 13000, Thailand
e-mail: adul_harn@yahoo.com

X. Wang and Z.M. Wang (eds.), *Nanoscale Thermoelectrics*, Lecture Notes in Nanoscale Science and Technology 16, DOI 10.1007/978-3-319-02012-9_10,

Since the combined approach of double filling and self-formed nanostructures could be applicable to various clathrate compounds, our results suggest a new strategy in the improvement of bulk TE materials.

10.1 Introduction

Thermoelectric (TE) materials can convert waste heat into electrical power, which is an effective way to reduce greenhouse gas emissions and contribute substantially to future power supply and sustainable energy management [1–6]. The main obstacle to the widespread use of TEs in diverse industries, e.g., for exhaust heat recovery in automobiles, is the low efficiency of materials in converting heat to electricity. The efficiency of a material used in TE devices is determined by the dimensionless figure of merit, $ZT = S^2T\rho^{-1}\kappa^{-1}$, where S is the Seebeck coefficient, T is the absolute temperature, ρ is the electrical resistivity, and κ is the total thermal conductivity ($\kappa = \kappa_{lat} + \kappa_{el}$, where κ_{lat} and κ_{el} are the lattice and electronic contributions, respectively). Since the S, ρ, and κ_{el} in bulk materials are interrelated, it is very difficult to control them independently. Therefore, the reduction of κ_{lat} is essential to enhancing ZT. The ZT value of the materials currently used in commercial cooling devices is still limited to about 1 or less over the entire operating temperature range, corresponding to a device efficiency of several percent. Recent improvements in TE materials have led to many advances, and enhanced ZT values have been reported for several classes of bulk materials, including filled skutterudites.

The name of skutterudite is derived from a naturally occurring mineral with $CoAs_3$ structure, which was firstly discovered in Skutterud (Norway). The general formula of skutterudite compounds is MX_3, where M is one of the group 9 transition metals such as Co, Rh, or Ir and X is a pnictogen atom such as P, As, and Sb. These compounds are body-centered-cubic structure that contains 32 atoms in the unit cell with space group Im3. The most important point of the skutterudite structure is that there are two voids in the unit cell which can be filled by filler atoms with an ionic radius lower than the cage radius. This generates a so-called filled skutterudite with formula RM_4X_{12}, where R is electropositive element like rare earth or alkaline earth. Figure 10.1 displays the filled skutterudite structure where the R, M, and X are shown in red, blue, and green spheres, respectively.

Early investigations on unfilled skutterudites dates back to the mid-1950s. Among skutterudites, $CoSb_3$ has attracted the greatest interest in waste heat to electricity conversion applications due to its reasonable band gap of ~0.2 eV, high carrier mobility, and the fact that it is composed of inexpensive and environmentally benign constituent elements as compared to other skutterudites such as $CoAs_3$. However, the κ_{lat} of the pure binary $CoSb_3$ is too high, which leads to low ZT and thus poor conversion efficiency for TE applications.

In 1977 La-filled [7] and in 1991 Ba-filled [8] skutterudites were synthesized. However, it has not become popular. In 1994, Slack [9] proposed the concept of "phonon–glass electron–crystal" (PGEC) as one of the desirable features a material

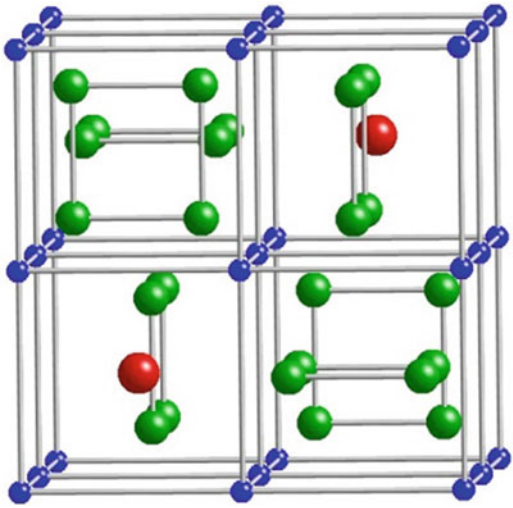

Fig. 10.1 Filled-skutterudite structure of RM_4X_{12}. R, M, and X are shown in *red*, *blue*, and *green* spheres, respectively

should possess to maximize the ZT, in which a material conducts heat like a glass but behaves like a good crystal for the electronic properties. The typical example of the PGEC concept is filled skutterudites, such as $CeFe_4Sb_{12}$ [10]. Filled skutterudites realize the PGEC concept through the following strategies: a semiconductor-like behavior may lead to large S and low ρ; in addition, the loosely bound filler atoms in the skutterudite cages act as rattlers and thereby reduce the κ_{lat} [11].

It has been reported that a large variety of guest atoms can be filled, such as rare earth elements [12–16], alkaline earth elements [17–19], alkali metals [20, 21], and others [22–26]. The filling atoms are loosely bound to the other atoms in the intrinsic cages, leading to strong phonon scattering and significant reduction of the κ_{lat} [27, 28]. In addition to the single-filled system, a double-filling approach has recently been attracting increasing attention. Introducing two filler types from different chemical groups into the cages of $CoSb_3$ could introduce two distinctive filler vibrational frequencies for a broader range lattice phonon scattering, leading to a further reduction of κ_{lat} [29, 30]. As the results, the maximum ZT values were improved to 1.3–1.4 in double-filled skutterudites as shown in Fig. 10.2 [12, 14, 16–21, 30–34].

As described above, it has been widely reported that the voids in $CoSb_3$ can be fully or partially filled with a variety of different atoms. However, reports on the TE properties of skutterudites filled by group 13 elements, such as Ga, In, and Tl, have been limited. Here we review the TE properties of $CoSb_3$-based skutterudites filled by group 13 elements, which are mainly obtained in our group. In particular, the TE properties of the single-filled system: $Tl_xCo_4Sb_{12}$ and $Ga_xCo_4Sb_{12}$ and the double-filled system: $Tl_{0.1}In_xCo_4Sb_{12}$ will be discussed.

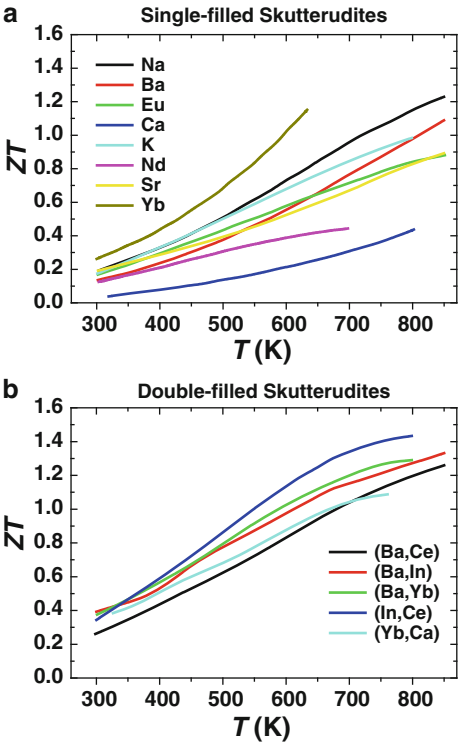

Fig. 10.2 Temperature dependence of dimensionless figure of merit, *ZT* of various filled-skutterudites reported so far; (**a**) single-filled system and (**b**) double-filled system

10.2 Thermoelectric Properties of Tl-filled skutterudite: $Tl_xCo_4Sb_{12}$ [26]

Among $CoSb_3$-based skutterudites filled by group 13 elements, the authors have focused on Tl-filled skutterudites: $Tl_xCo_4Sb_{12}$, because of the following reasons. First, the electronegativity of Tl is close to that of Sb, which suggests that it may have a small effect on the electrical transport properties of $CoSb_3$. Second, the radius of the void in a 12-coordinated site is close to the radius of Tl^{1+}. Finally, Tl is heavier than other elements that have been recognized as compatible *R* atoms in RCo_4Sb_{12}. However, there is only one report [22], of Tl-filled skutterudites in which the TE properties below room temperature have been systematically investigated. In addition, in [22], it has been reported that Tl-filled skutterudites readily formed and up to around 22 % of the voids in $CoSb_3$ could be filled with Tl. Therefore, the authors prepared the polycrystalline samples of $Tl_xCo_4Sb_{12}$ ($x = 0$, 0.05, 0.10, 0.15, 0.20, and 0.25) and examined their high-temperature TE properties from room temperature to 750 K [26].

Figure 10.3 shows powder x-ray diffraction (XRD) patterns of the polycrystalline samples of $Tl_xCo_4Sb_{12}$ ($x = 0, 0.05, 0.10, 0.15, 0.20$, and 0.25) prepared in our group, together with the peak positions calculated from the crystal structure of $CoSb_3$.

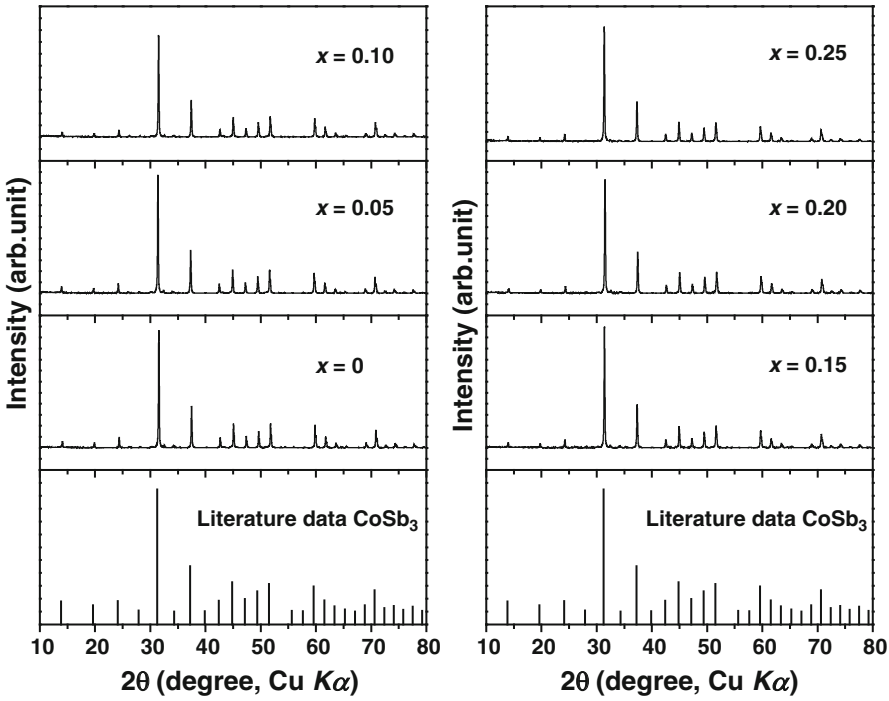

Fig. 10.3 Powder XRD patterns of polycrystalline samples of $Tl_xCo_4Sb_{12}$ ($x = 0$, 0.05, 0.10, 0.15, 0.20, and 0.25), together with the peak positions calculated from the crystal structure of $CoSb_3$

Basically, all samples are identified as skutterudite compounds, although they contain negligible amounts of $CoSb_2$ as an impurity phase. The lattice parameters of $Tl_xCo_4Sb_{12}$ increase almost linearly with the increase in the Tl content up to $x = 0.20$ and the lattice parameter of $Tl_{0.25}Co_4Sb_{12}$ is almost identical with that of $Tl_{0.20}Co_4Sb_{12}$, as shown in Fig. 10.4. Therefore, it can be concluded that the Tl-filling limit in $CoSb_3$ is between 20 and 25 at.%, which is consistent with the literature data [22].

Figure 10.5 shows the temperature dependence of (a) the electrical resistivity, ρ and (b) Seebeck coefficient, S for polycrystalline samples of $Tl_xCo_4Sb_{12}$. The magnitude of ρ for $CoSb_3$ is approximately 11×10^{-5} Ω m at 330 K and decreases with increasing temperature. On the other hand, the ρ values of $Tl_xCo_4Sb_{12}$ are rather low ($1–3 \times 10^{-5}$ Ω m at 330 K) and indicate slight-positive temperature dependency. The magnitude of ρ for $Tl_xCo_4Sb_{12}$ decreases with increase in the Tl content x. S for all samples is negative, which indicates that a majority of charge carriers are electrons. The absolute S of $CoSb_3$ is 330 μV K^{-1} at 330 K and remains constant up to around 450 K, then decreases gradually with increasing temperature. The absolute S of $Tl_xCo_4Sb_{12}$ decreases with increase in the Tl content x. The results for both ρ and S imply that Tl-filling leads to an increase of the electron

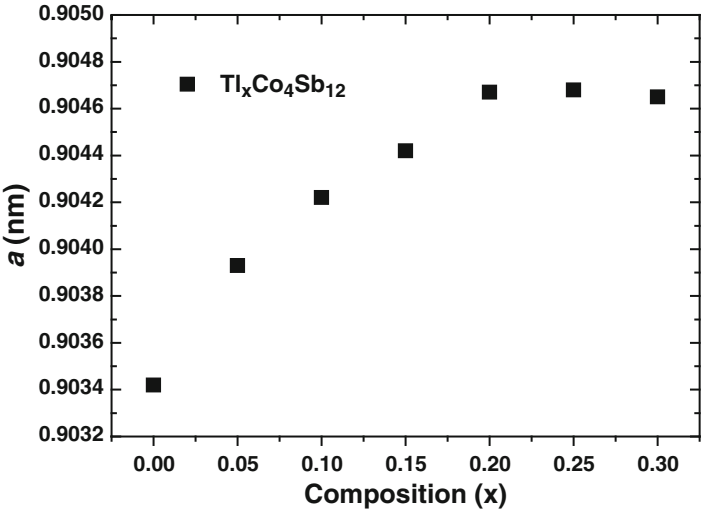

Fig. 10.4 Lattice parameters of polycrystalline samples of $Tl_xCo_4Sb_{12}$ ($x = 0$, 0.05, 0.10, 0.15, 0.20, and 0.25)

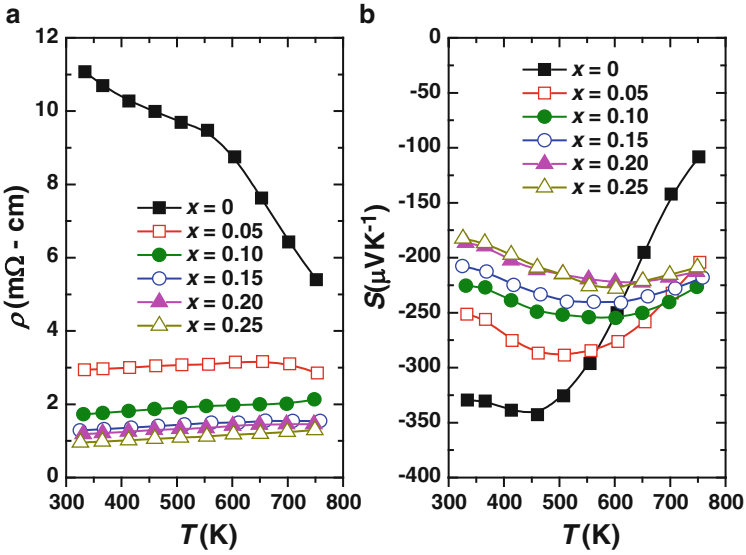

Fig. 10.5 Temperature dependences of (**a**) the electrical resistivity, ρ and (**b**) the Seebeck coefficient, S of polycrystalline samples of $Tl_xCo_4Sb_{12}$ ($x = 0$, 0.05, 0.10, 0.15, 0.20, and 0.25)

carrier concentration. Room temperature values of Hall carrier concentration (n_H) and Hall mobility (μ_H) for $Tl_xCo_4Sb_{12}$ are summarized in Table 10.1 and plotted in Fig. 10.6, as a function of the Tl content x. n_H for $Tl_xCo_4Sb_{12}$ increases with increasing Tl content, viz. n_H for $Tl_{0.25}Co_4Sb_{12}$ (23.9×10^{-19} cm^{-3}) is more than

Table 10.1 Lattice parameter a, density d, Seebeck coefficient S (300 K), electrical resistivity ρ (300 K), Hall carrier concentration n_H (300 K), Hall mobility μ_H (300 K), average sound velocity v_{ave}, Young's modulus E, and Debye temperature θ_D for polycrystalline samples of $Tl_xCo_4Sb_{12}$ ($x = 0$, 0.05, 0.10, 0.15, 0.20, and 0.25)

x	a (nm)	d (g cm^{-3})	% T.D.	S (μV K^{-1})	ρ (mΩ cm)	n_H (10^{19} cm^{-3})	μ_H (cm^2 V^{-1} s^{-1})	v_{ave} (m s^{-1})	E (GPa)	θ_D (K)
0	0.90342	7.55	98	−333	13.76	1.56	29.02	3,684	142	320
0.05	0.90393	7.62	99	−241	2.98	5.89	35.50	3,710	146	321
0.10	0.90422	7.59	98	−221	1.80	10.60	32.73	3,695	144	320
0.15	0.90442	7.71	99	−205	1.25	18.10	27.50	3,666	143	318
0.20	0.90467	7.69	98	−180	1.11	21.10	26.65	3,637	140	315
0.25	0.90468	7.69	98	−184	1.00	23.90	26.10	3,613	139	313

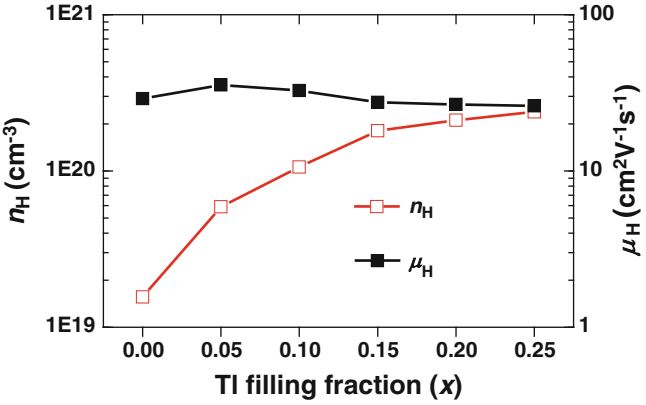

Fig. 10.6 The Hall carrier concentration, n_H and Hall mobility, μ_H at 300 K of polycrystalline samples of $Tl_xCo_4Sb_{12}$, as a function of the Tl filling fraction, x

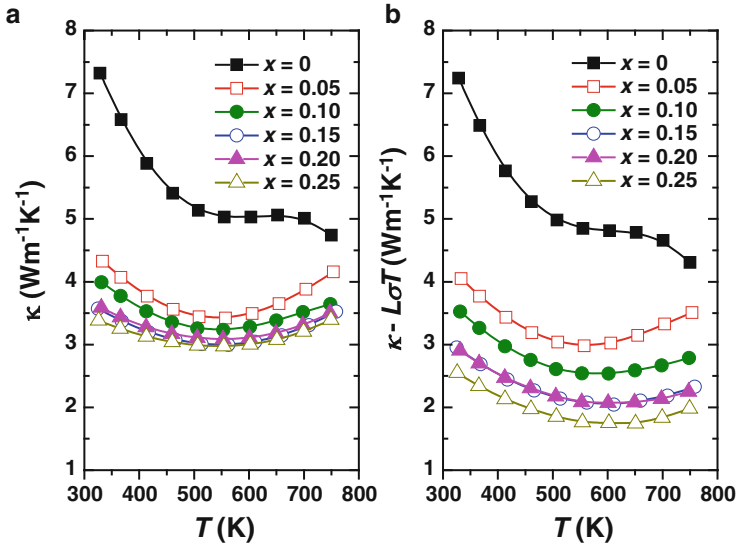

Fig. 10.7 Temperature dependences of the thermal conductivity of polycrystalline samples of $Tl_xCo_4Sb_{12}$ ($x = 0$, 0.05, 0.10, 0.15, 0.20, and 0.25); (**a**) total thermal conductivity, κ and (**b**) lattice thermal conductivity, κ_{lat}

ten times that of $CoSb_3$ (1.56×10^{-19} cm^{-3}). On the other hand, the $Tl_xCo_4Sb_{12}$ samples exhibits similar μ_H values at all Tl-filling contents. These results indicate that the Tl-filling increases the n_H, but has no significant influence on μ_H.

The thermal conductivity (κ) for $Tl_xCo_4Sb_{12}$ are significantly reduced by Tl-filling, as shown in Fig. 10.7a. $Tl_{0.25}Co_4Sb_{12}$ exhibits the lowest κ over the entire temperature range; at room temperature, κ for $Tl_{0.25}Co_4Sb_{12}$ is 3.4 W m^{-1} K^{-1}, which is less than

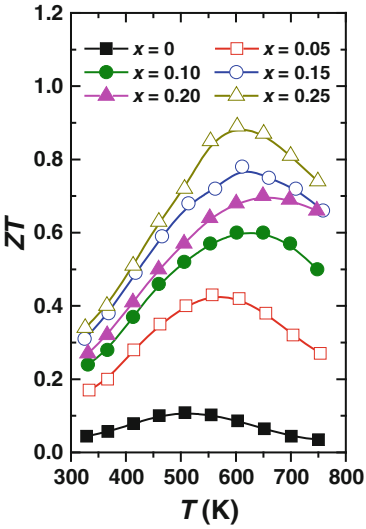

Fig. 10.8 Temperature dependences of the dimensionless figure of merit, *ZT* of polycrystalline samples of $Tl_xCo_4Sb_{12}$ ($x = 0$, 0.05, 0.10, 0.15, 0.20, and 0.25)

half that of $CoSb_3$. Figure 10.7b shows the temperature dependence of the lattice thermal conductivity (κ_{lat}) for $Tl_xCo_4Sb_{12}$. κ_{lat} was obtained by subtracting the electronic thermal conductivity ($\kappa_{el} = L\sigma T$, $L = 2.45 \times 10^{-8}$ W Ω K^{-2}) from the total (measured) thermal conductivity κ. κ_{lat} for $Tl_xCo_4Sb_{12}$ significantly decreases with increase in the Tl content. However, as summarized in Table 10.1, the experimental results for average sound velocity (v_{ave}), Young's modulus (E), and Debye temperature (θ_D) obtained from the sound velocity measurements are similar at all Tl-filling contents, despite κ_{lat} being significantly reduced by Tl-filling. These results imply that Tl in $CoSb_3$ has no direct effect on the strength of the interatomic bonding, but that Tl is weakly bonded with the other atoms, which results in a reduction of κ_{lat} by rattling within the cage.

The low κ, compared with $CoSb_3$, results in large TE figure of merit (*ZT*) for Tl-filled $CoSb_3$, as shown in Fig. 10.8. In particular, $Tl_{0.25}Co_4Sb_{12}$ exhibits the best *ZT* values; the maximum value of 0.90 is obtained at 600 K.

10.3 Thermoelectric Properties of Ga-Filled Skutterudite: $Ga_xCo_4Sb_{12}$ [35]

There have been various reports on the TE properties of skutterudites filled by various elements, such as Ba-, K-, Na-, Ca-, Nd-, Sr-, Eu-, Yb-, In-, and Tl-filled skutterudites [12, 14, 16–22, 26, 36–38]. Although the TE properties of In-, and Tl-filled skutterudites have been investigated, the Ga-$CoSb_3$ system has been scarcely investigated. Recently, Xiong et al. [39] has reported the TE properties of the $Yb_{0.26}Co_4Sb_{12}/y$GaSb system, where only very small amount of Ga can fill

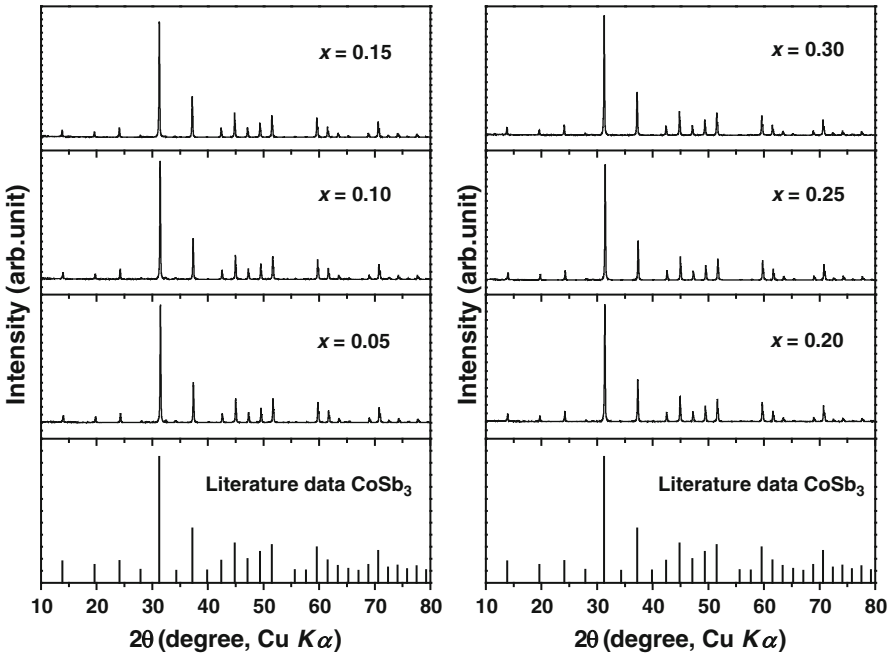

Fig. 10.9 Powder XRD patterns of polycrystalline samples of $Ga_xCo_4Sb_{12}$ ($x = 0.05$, 0.10, 0.15, 0.20, 0.25, and 0.30), together with the peak positions calculated from the crystal structure of $CoSb_3$

into the crystal voids of $CoSb_3$. Additionally, very recently, Qiu has reported that Ga atoms occupy both the void and Sb sites in $CoSb_3$ and couple with each other and the *ZT* quickly increases to 0.7 at a Ga doping content as low as 0.1 per Co_4Sb_{12} [40]. Here, the authors show the TE properties of polycrystalline samples of $Ga_xCo_4Sb_{12}$ ($x = 0.05$, 0.10, 0.15, 0.20, 0.25, and 0.30) in the temperature range from room temperature to 750 K, which are obtained in the author's group [35].

The powder XRD patterns of the polycrystalline samples of $Ga_xCo_4Sb_{12}$ ($x = 0.05$, 0.10, 0.15, 0.20, 0.25, and 0.30) are shown in Fig. 10.9. All the peaks in the XRD patterns are identified as the peaks derived from the skutterudite phase. However, in the XRD patterns of the samples of $x = 0.05$, 0.10, and 0.15, negligible peaks of $CoSb_2$ as the impurity phase can be observed. The lattice parameters calculated from the XRD patterns are plotted in Fig. 10.10, together with the data for Tl-filled $CoSb_3$ [26]. The lattice parameters of the Ga-$CoSb_3$ samples slightly increase with Ga-addition up to around $x = 0.05$, and after that keep a constant. In contrast, the lattice parameters of the Tl-$CoSb_3$ samples increase almost linearly with increasing Tl-addition up to $x = 0.20$ and after that keep a constant. These results imply that Tl can be filled up to around $x = 0.20$ in $Tl_xCo_4Sb_{12}$ but the maximum filling ratio of Ga in $CoSb_3$ is lower than $x = 0.05$ in $Ga_xCo_4Sb_{12}$. This result is well consistent with the other Ga-filled skutterudite reported by Xiong et al. [39], in which

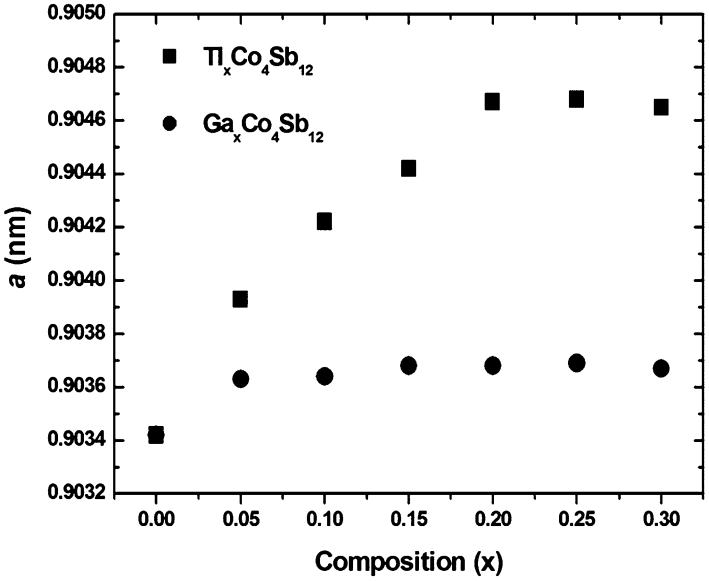

Fig. 10.10 Lattice parameters of polycrystalline samples of $Ga_xCo_4Sb_{12}$ ($x = 0.05$, 0.10, 0.15, 0.20, 0.25, and 0.30), together with the data of polycrystalline samples of $Tl_xCo_4Sb_{12}$

only very small amount of Ga can fill into the crystal voids of $CoSb_3$. In addition, in [40], it has been reported that the maximum filling fraction of Ga in the voids of $CoSb_3$ is around 8 %.

In order to confirm the filling limit of Ga into $CoSb_3$, the field emission scanning electron microscopy (FE-SEM) and energy dispersive x-ray (EDX) analysis was performed on the surface of the hot-pressed samples. The XRD pattern, FE-SEM image, and EDX mapping images of $Ga_{0.30}Co_4Sb_{12}$ are shown in Fig. 10.11. As shown in Fig. 10.11a, no peaks corresponding to GaSb are observed in the XRD pattern. Since the main peak position of Ga metal is close to a peak of $CoSb_3$, it is unclear that whether Ga metal exists or not in the sample. On the other hand, as shown in Fig. 10.11b, the area that Ga concentrated in small pores is observed in the FE-SEM image and the EDX mapping images. Therefore, it can be concluded that most of Ga exists as metal state in the $Ga_{0.30}Co_4Sb_{12}$ sample. This result is not consistent with the other Ga-filled skutterudite reported by Xiong et al. [39], in which some evidence of impurity phase of GaSb but not metallic Ga has been shown. At this point, the reason of the differences between our data and the literature data has not been clearly understood. From the quantitative EDX analysis, the amount of Ga in the matrix phase is confirmed to be approximately 0.1 at.%, i.e., $x = \sim 0.02$ in $Ga_xCo_4Sb_{12}$. Therefore, it can be said that the maximum filling ratio of Ga into $CoSb_3$ is $x = 0.02$ in $Ga_xCo_4Sb_{12}$, and when exceeding the filling limit, Ga exists as metal state. This is clearly different from the cases of In- and Tl-filled $CoSb_3$, in which both In and Tl can be filled up to approximately $0.05 < x < 0.1$ in

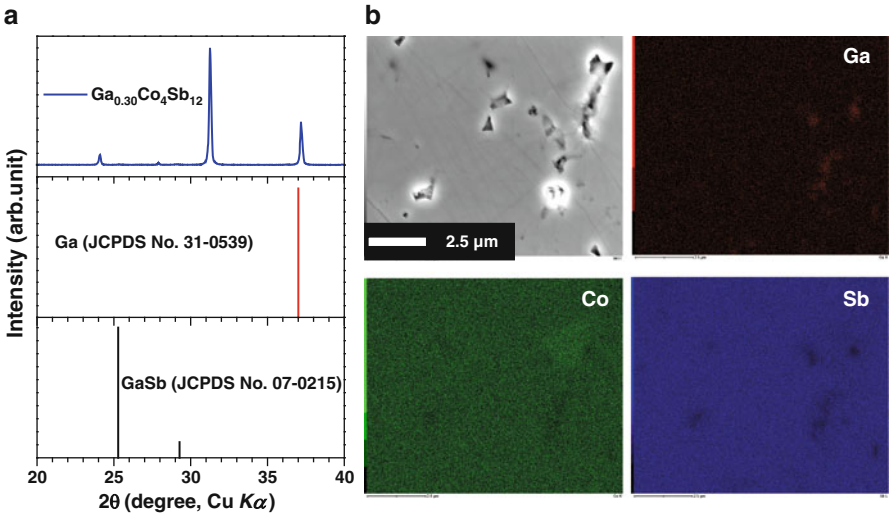

Fig. 10.11 (**a**) Powder XRD pattern of polycrystalline sample of $Ga_{0.30}Co_4Sb_{12}$, together with the peak positions of Ga and GaSb. (**b**) SEM and EDX mapping images of polycrystalline sample of $Ga_{0.30}Co_4Sb_{12}$

$In_xCo_4Sb_{12}$ [41] and $x = 0.2$ in $Tl_xCo_4Sb_{12}$ [26], respectively. The Ga metal may exist as liquid phase during high-temperature TE properties measurements.

In order to verify the maximum filling limit of Ga and Tl into $CoSb_3$, we performed low-temperature heat capacity analyses on the Co_4Sb_{12}, $Ga_{0.2}Co_4Sb_{12}$, and $Tl_{0.2}Co_4Sb_{12}$ samples. At low temperature (below 7 K), standard plots of C_P/T versus T^2 was linear for Co_4Sb_{12} sample and yielded Debye temperature of 306 K. This result is well consistent with the literature value (307 K for single crystals of Co_4Sb_{12} reported by Caillat et al. [42]). The contribution of the filling atoms to the heat capacity would emerge as a form of excess heat capacity (ΔC). In the present case, we considered the following two values of ΔC: $\Delta C_1 = C$ of $Ga_{0.2}Co_4Sb_{12} - C$ of Co_4Sb_{12}, and $\Delta C_2 = C$ of $Tl_{0.2}Co_4Sb_{12} - C$ of Co_4Sb_{12}. Figures 10.12 and 10.13 plot ΔC_1 and ΔC_2 as a function of temperature, respectively. ΔC is well approximated by an Einstein contribution:

$$\Delta C = C_E(T) = 3Ry\left(\frac{\theta_E}{T}\right)^2 \frac{\exp(\theta_E/T)}{(\exp(\theta_E/T)-1)^2}, \tag{10.1}$$

where R is the gas constant, y is the content of the filling atom in the formula of $Ga_yCo_4Sb_{12}$ or $Tl_yCo_4Sb_{12}$, and θ_E is the Einstein temperature. Below 20 K, both ΔC_1 and ΔC_2 are well described by (10.1), in which we set two unknown parameters: y and θ_E. In the case of ΔC_1, y and θ_E were found to be 0.02 and 35 K, respectively. On the other hand, in the case of ΔC_2, y and θ_E were found to be 0.15 and 56 K, respectively. Thus, it can be said that Ga or Tl can be filled up to $y = 0.02$

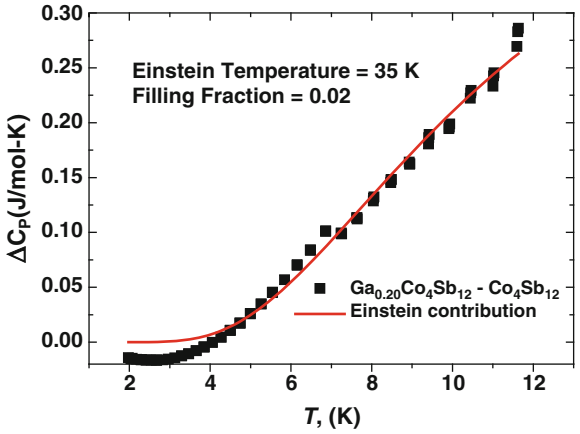

Fig. 10.12 The difference in the heat capacities between $Ga_{0.2}Co_4Sb_{12}$ and Co_4Sb_{12}, together with a line fitted by using the Einstein model

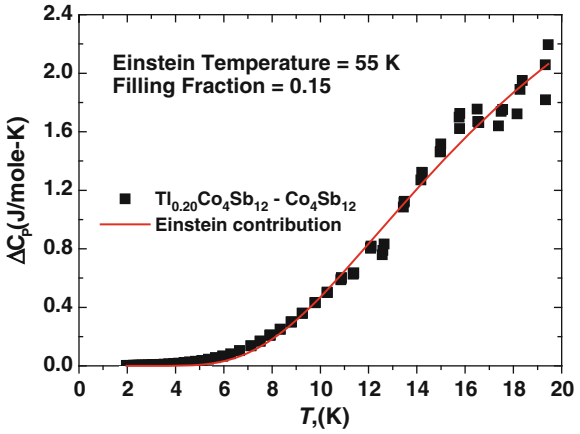

Fig. 10.13 The difference in the heat capacities between $Tl_{0.2}Co_4Sb_{12}$ and Co_4Sb_{12}, together with a line fitted by using the Einstein model

in $Ga_yCo_4Sb_{12}$ and $y = 0.15$ in $Tl_yCo_4Sb_{12}$, respectively. Note that the obtained Einstein temperature of 56 K is close to the value of 52 K estimated from the atomic displacement parameters for $Tl_{0.22}Co_4Sb_{12}$ [22] indicating the substantial rattling of Tl in the skutterudite structure. Similarly, in the case of Ga-$CoSb_3$ system, the maximum filling limit was calculated to be $y = 0.02$ in $Ga_yCo_4Sb_{12}$, well consistent with the XRD and FE-SEM/EDX results as described above.

Temperature dependences of the electrical resistivity (ρ) and the Seebeck coefficient (S) of the polycrystalline samples of $Ga_xCo_4Sb_{12}$ ($x = 0.05, 0.10, 0.15, 0.20, 0.25$, and 0.30) are shown in Fig. 10.14a, b, respectively. The ρ of all the samples decrease with temperature, showing semiconductor behavior. By adding Ga to $CoSb_3$, the ρ values increase with increasing x up to $x = 0.15$, and then decrease. The S values are negative for all the samples, indicating that the majority of charge carriers are electrons. The absolute S of all the samples are almost constant up to

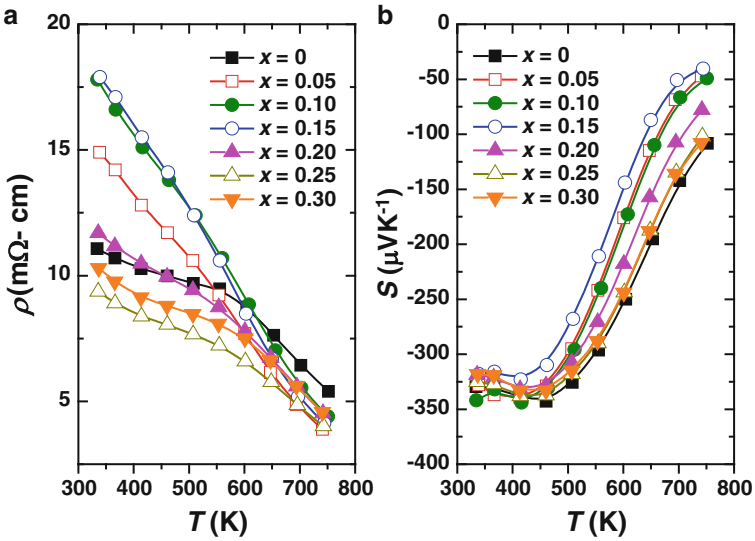

Fig. 10.14 Temperature dependences of (**a**) the electrical resistivity, ρ and (**b**) the Seebeck coefficient, S of polycrystalline samples of $Ga_xCo_4Sb_{12}$ (x = 0.05, 0.10, 0.15, 0.20, 0.25, and 0.30)

Table 10.2 Lattice parameter a, sample bulk density d, Hall carrier concentration n_H (300 K), and Hall mobility μ_H (300 K) for polycrystalline samples of $Ga_xCo_4Sb_{12}$ (x = 0.05, 0.10, 0.15, 0.20, 0.25, and 0.30)

x	a (nm)	d (g cm^{-3})	n_H (10^{19} cm^{-3})	μ_H (cm^2 V^{-1} s^{-1})
0.05	0.90363	7.65	1.51	27.8
0.10	0.90364	7.65	1.07	31.9
0.15	0.90368	7.64	2.06	24.5
0.20	0.90368	7.66	2.67	19.9
0.25	0.90369	7.63	3.42	15.9
0.30	0.90367	7.64	3.33	15.0

around 500 K, and decrease rapidly with increasing temperature, which is due to the thermal excitation of the charge carriers. At around room temperature, all the samples show the similar S values. However, at high temperatures, the absolute S decrease with increasing x in $Ga_xCo_4Sb_{12}$ up to x = 0.15, and then increase. As summarized in Table 10.2, the n_H slightly increases with increasing the amount of Ga, while the μ_H decreases, which is due to the combination of the Ga-filling into the voids in the $CoSb_3$ crystal and precipitation of Ga metal. In contrast to the Tl-filled $CoSb_3$, the n_H of the Ga-added $CoSb_3$ is not sufficiently increased because only a few Ga is filled into $CoSb_3$. The n_H of $Tl_{0.25}Co_4Sb_{12}$ is 23.90 $\times$ 10^{19} cm^{-3} [26], which is almost ten times larger than that of $Ga_{0.25}Co_4Sb_{12}$ (3.42 $\times$ 10^{19} cm^{-3}).

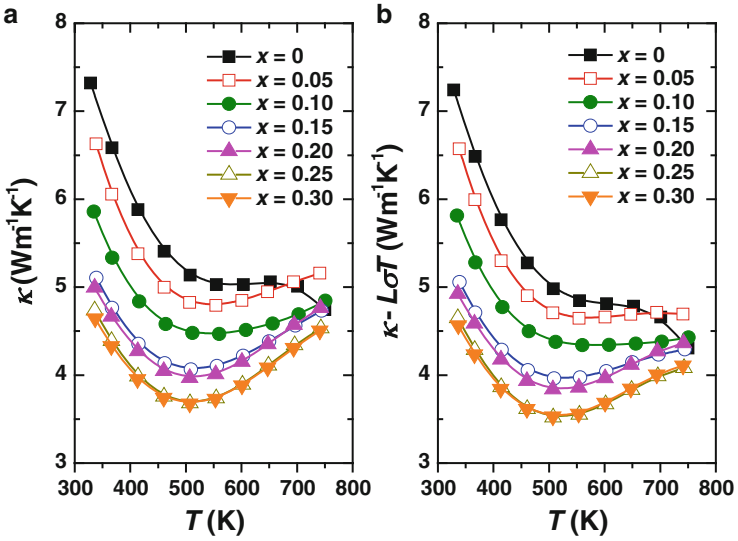

Fig. 10.15 Temperature dependences of the thermal conductivity of polycrystalline samples of $Ga_xCo_4Sb_{12}$ ($x = 0.05, 0.10, 0.15, 0.20, 0.25$, and 0.30); (**a**) total thermal conductivity, κ and (**b**) lattice thermal conductivity, κ_{lat}

Temperature dependences of the κ and the κ_{lat} for polycrystalline samples of $Ga_xCo_4Sb_{12}$ ($x = 0.05, 0.10, 0.15, 0.20, 0.25$, and 0.30) are shown in Fig. 10.15a, b, respectively. The κ decreases with increasing temperature first and then increases from around 550 K. This temperature dependence can be attributed to a bipolar conduction in semiconductors. The κ_{lat} of $Ga_xCo_4Sb_{12}$ drastically decreases with Ga-addition. $Ga_{0.25}Co_4Sb_{12}$ exhibits the lowest κ_{lat} (3.52 W m^{-1} K^{-1} at 500 K). These results imply that not only the filled Ga but also the precipitated Ga lead to the effective reduction of κ_{lat}.

Temperature dependence of the ZT for polycrystalline samples of $Ga_xCo_4Sb_{12}$ ($x = 0.05, 0.10, 0.15, 0.20, 0.25$, and 0.30) is shown in Fig. 10.16. Although Ga can be filled only up to $x = \sim 0.02$ in $Ga_xCo_4Sb_{12}$, significant reduction of κ_{lat} is achieved, leading to enhancement of ZT. In particular, $Ga_{0.25}Co_4Sb_{12}$ exhibits the maximum ZT value of 0.18 at around 500 K. This value is lower than those of In- and Tl-filled skutterudites [22, 26, 37, 38]. This low ZT of the Ga-$CoSb_3$ system is likely due to the unoptimized carrier concentration. In case of the Tl-$CoSb_3$ system, the Tl-filling into $CoSb_3$ increases carrier concentration [26]. However, in case of the Ga-$CoSb_3$ system, the carriers are not sufficiently doped because only a few Ga is filled into $CoSb_3$. Nonetheless, since Ga-adding to $CoSb_3$ is effective method for reduction of κ_{lat}.

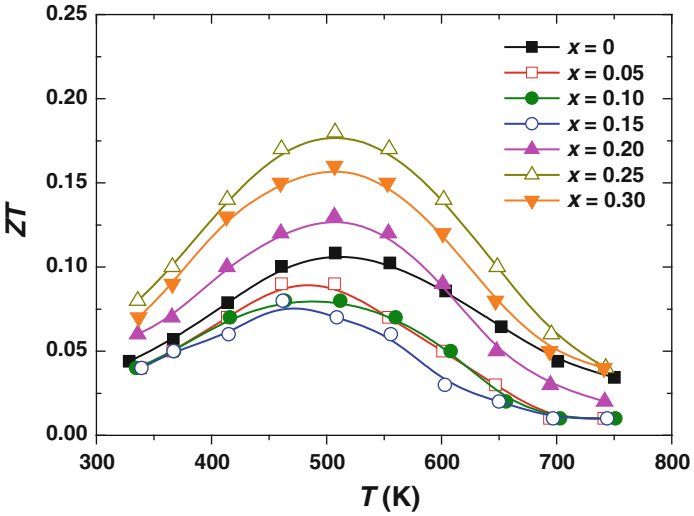

Fig. 10.16 Temperature dependences of the dimensionless figure of merit, *ZT* of polycrystalline samples of $Ga_xCo_4Sb_{12}$ ($x = 0.05$, 0.10, 0.15, 0.20, 0.25, and 0.30)

10.4 Thermoelectric Properties of Tl- and In Double-Filled Skutterudite: $Tl_{0.1}In_xCo_4Sb_{12}$ [43]

Skutterudites filled by group 13 elements, of Ga-, In-, and Tl-filled systems, have attracted much attention recently as high-performance TE materials. Among the compounds in the Tl-filled system, our group has examined the high-temperature TE properties of $Tl_yCo_4Sb_{12}$ and obtained a maximum *ZT* of 0.90 at 600 K for $Tl_{0.25}Co_4Sb_{12}$ [26]. The maximum *ZT* values for In- and Tl-filled skutterudites have been obtained at the compositions of the maximum filling limit [26, 37]. Thus, the enhancement of the *ZT* of these filled skutterudites is restricted by the filling limit of atoms into the voids of the skutterudite structure. In the case of In-filled skutterudites, there are a few reports in which In naturally forms nano-sized InSb inclusions when it exceeds the filling limit, and these nano-inclusions appear to play an important role in significantly reducing κ_{lat} [34, 44]. However, there have been a number of reports where no such nano-inclusions were observed in the same In-filled system [38, 45]. Thus, it remains unclear whether any nanostructures form in In-filled skutterudites.

Here, we review the results on the dramatically reduced κ_{lat}, and thus enhanced *ZT*, for $CoSb_3$-based skutterudites by a combined approach of double filling of group 13 elements (Tl and In) and self-forming of nanostructures [43].

In the XRD patterns of polycrystalline samples of $Tl_{0.1}In_xCo_4Sb_{12}$ ($x = 0.1$, 0.2, and 0.3), all the peaks indicate a skutterudite structure with the space group *Im*3, and there are no notable peaks corresponding to impurities as shown in Fig. 10.17. The XRD patterns confirm that all samples have nearly the same lattice parameter

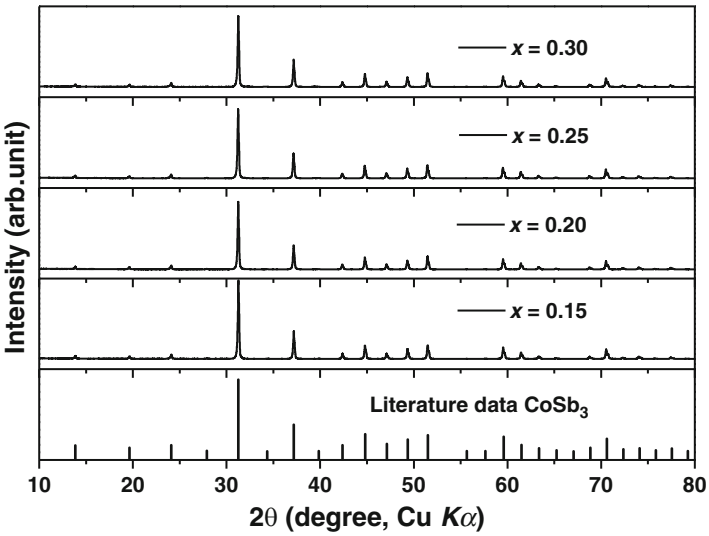

Fig. 10.17 Powder XRD patterns of polycrystalline samples of $Tl_{0.1}In_xCo_4Sb_{12}$ ($x = 0.15$, 0.20, 0.25, and 0.30), together with the peak positions calculated from the crystal structure of $CoSb_3$

Table 10.3 Lattice parameter a, sample bulk density d, Hall carrier concentration n_H (300 K), and Hall mobility μ_H (300 K) for polycrystalline samples of $Tl_{0.1}In_xCo_4Sb_{12}$ ($x = 0.15$, 0.20, 0.25, and 0.30)

x	a (nm)	d (g cm^{-3})	n_H (10^{19} cm^{-3})	μ_H (cm^2 V^{-1} s^{-1})
0.15	0.9047	7.75	23.61	35.21
0.20	0.9048	7.76	34.17	28.01
0.25	0.9048	7.78	34.13	27.43
0.30	0.9049	7.76	40.00	25.03

values, as summarized in Table 10.3. According to Vegard's rule, under the assumption that Tl is fully filled while In is partly filled, the lattice parameter a of $Tl_{0.1}In_xCo_4Sb_{12}$ can be written as:

$$a \text{ of } Tl_{0.1}In_xCo_4Sb_{12} = a \text{ of } Co_4Sb_{12} + \Delta a_1 + \Delta a_2, \tag{10.2}$$

where a of Co_4Sb_{12} is 0.9034 nm [26], $\Delta a_1 = a$ of $Tl_{0.1}Co_4Sb_{12} - a$ of Co_4Sb_{12}, and $\Delta a_2 = a$ of $In_xCo_4Sb_{12} - a$ of Co_4Sb_{12}. The values of Δa_1 and Δa_2 can be calculated from the changes in the lattice parameters of Tl- and In-filled $CoSb_3$ using the filling ratio obtained by the present authors' group. By fitting the calculated lattice parameter to the experimental one, we obtained $x = 0.09$. This indicates that the maximum filling limits of Tl and In in $Tl_{0.1}In_xCo_4Sb_{12}$ are 0.1 and 0.09, respectively. Therefore, it is believed that a secondary phase composed mainly of In may exist in addition to the skutterudite phase after exceeding the maximum filling limit of In.

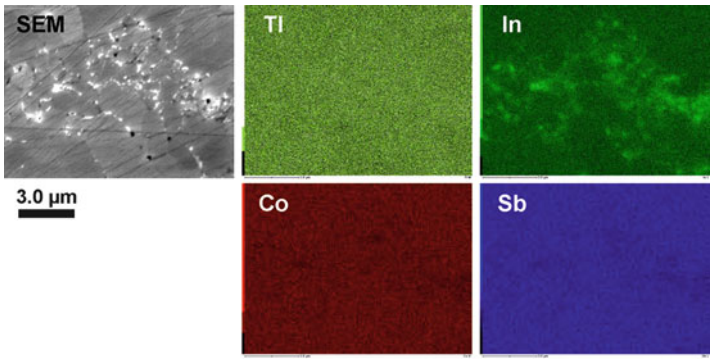

Fig. 10.18 FE-SEM and EDX mapping images of the polycrystalline sample of $Tl_{0.1}In_{0.3}Co_4Sb_{12}$

The FE-SEM and EDX mapping images of the hot-pressed $Tl_{0.1}In_{0.3}Co_4Sb_{12}$ sample are shown in Fig. 10.18. In these images, an In-rich region can be clearly observed mainly at the grain boundaries, implying that In added after exceeding the maximum filling limit precipitates as a secondary phase. Since the particle size of the secondary phase is too small, the peaks of this impurity phase cannot be observed in the XRD patterns.

In order to identify the chemical state of the In-based secondary phase, we performed transmission electron microscopy (TEM) and X-ray absorption fine structure (XAFS) analyses on the $Tl_{0.1}In_{0.3}Co_4Sb_{12}$ sample. TEM image taken from a single grain of a sintered pellet of $Tl_{0.1}In_{0.3}Co_4Sb_{12}$ is shown in Fig. 10.19a. Nanoparticles (<50 nm) can be clearly observed. They have mostly formed along the grain boundaries. It is thought that they are composed mainly of In present in excess of its filling limit. The nanoparticles were analyzed by electron diffraction techniques. The electron diffraction patterns obtained are shown in Fig. 10.19b, c. The incident beam was focused to a diameter of ~10 nm. The electron diffraction patterns are entirely consistent with In_2O_3 (space group: Ia-3) viewed along the [110] and [112] directions.

To identify the chemical state of In within the sample, In L_3-edge x-ray absorption near edge structure (XANES) measurements were performed on a $Tl_{0.1}In_{0.3}Co_4Sb_{12}$ bulk sample at the Synchrotron Light Research Institute, Thailand. Figure 10.19d compares the measured In L_3-edge spectra of this $Tl_{0.1}In_{0.3}Co_4Sb_{12}$ bulk sample and the reference In metal and In_2O_3 powder. Clearly, all the features of the XANES In L_3-edge spectrum of the $Tl_{0.1}In_{0.3}Co_4Sb_{12}$ bulk sample agree very well with those of the reference In_2O_3 powder. This indicates that the In added in excess of the filling limit within the sample is in the form of In_2O_3. Thus, the XANES measurements confirm that the $Tl_{0.1}In_{0.3}Co_4Sb_{12}$ sample contains In_2O_3.

Temperature dependences of the electrical resistivity (ρ) and the Seebeck coefficient (S) of the polycrystalline samples of $Tl_{0.1}In_xCo_4Sb_{12}$ ($x = 0.15$, 0.20, 0.25, and 0.30) are shown in Fig. 10.20a, b, respectively. The ρ of all the samples decrease dramatically with In-addition. By adding Tl and In to $CoSb_3$, the ρ values

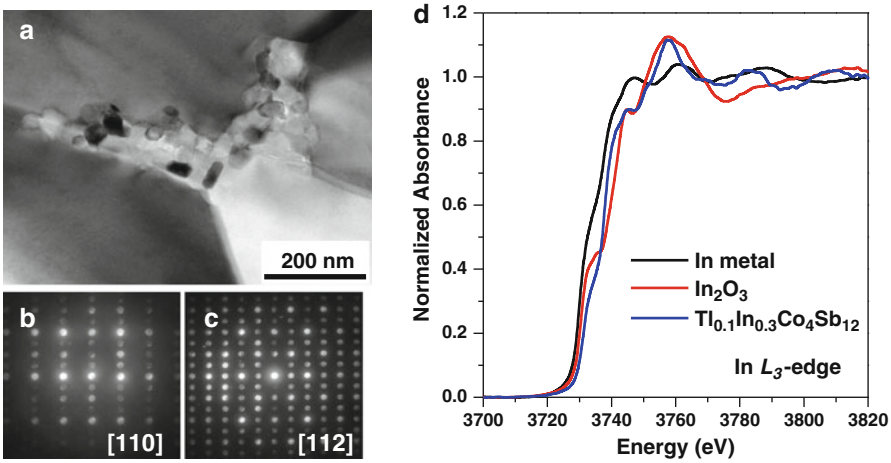

Fig. 10.19 (**a**) TEM image taken from a single grain of the sintered pellet of $Tl_{0.1}In_{0.3}Co_4Sb_{12}$; (**b**) and (**c**) electron diffraction patterns obtained with the electron beam aligned along the [110] and [112] directions, respectively; (**d**) comparison of the measured In L3-edge normalized spectra of a $Tl_{0.1}In_{0.3}Co_4Sb_{12}$ bulk sample with the reference In metal and In_2O_3 powder

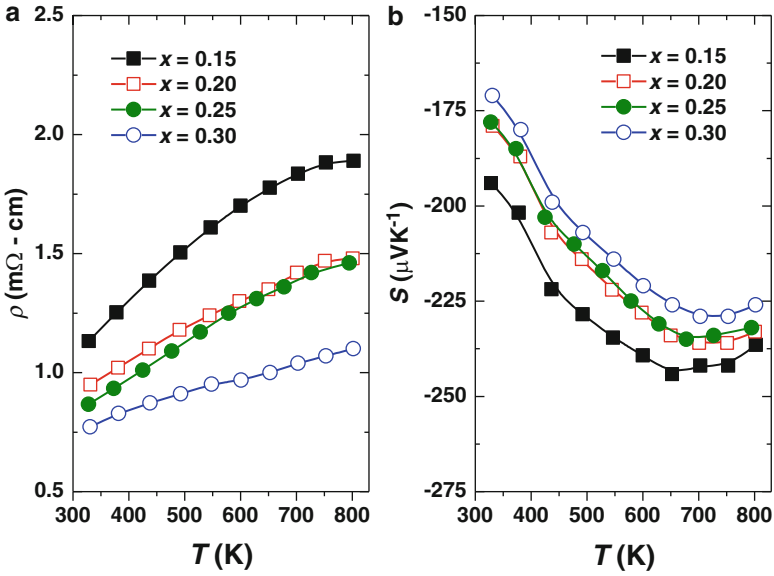

Fig. 10.20 Temperature dependences of (**a**) the electrical resistivity, ρ and (**b**) the Seebeck coefficient, S of polycrystalline samples of $Tl_{0.1}In_xCo_4Sb_{12}$ ($x = 0.15$, 0.20, 0.25, and 0.30)

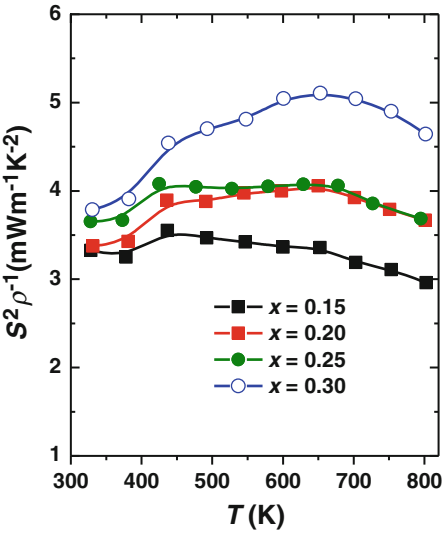

Fig. 10.21 Temperature dependences of the power factor, $S^2\rho^{-1}$ of polycrystalline samples of $Tl_{0.1}Tl_xCo_4Sb_{12}$ ($x = 0.15$, 0.20, 0.25, and 0.30)

of all the samples are below $1.25 \times 10^{-5}\ \Omega$ m at room temperature and increase with elevated temperature, typical of heavily doped semiconductors. The $Tl_{0.1}In_{0.3}Co_4Sb_{12}$ sample exhibits the lowest ρ value, $7.5 \times 10^{-6}\ \Omega$ m at room temperature. The S values are negative for all the samples, indicating that the majority of charge carriers are electrons. The absolute S of all the samples increases up to around 700 K, and decreases with increasing temperature. As summarized in Table 10.3, there is a large increase in n_H, while μ_H shows a minimal increase with increasing total filling fraction, which means that Tl/In addition leads to a net increase in conduction electrons but has no significant influence on the scattering of carriers. As shown in Fig. 10.21, all the samples show the constant and large values of the power factor ($S^2\rho^{-1}$) in the whole temperature range investigated in the present study. The $Tl_{0.1}In_{0.3}Co_4Sb_{12}$ sample exhibits the highest power factor, around 5.0 mW m^{-1} K^{-2} in relatively wide temperature range from 600 to 750 K.

Temperature dependences of the κ and the κ_{lat} for polycrystalline samples of $Tl_{0.1}In_xCo_4Sb_{12}$ ($x = 0.15$, 0.20, 0.25, and 0.30) are shown in Fig. 10.22a, b, respectively. The κ decreases with increasing temperature first and then increases from around 600 to 700 K. This temperature dependence can be attributed to a bipolar conduction in semiconductors. The κ_{lat} of $Tl_{0.1}In_xCo_4Sb_{12}$ drastically decreases with In-addition due to the phonon scattering by Tl- and In-rattling and nano-sized In_2O_3 precipitated at grain boundaries.

The temperature dependences of the κ_{lat} of polycrystalline samples of $CoSb_3$, $Tl_{0.1}Co_4Sb_{12}$, $Tl_{0.1}In_{0.1}Co_4Sb_{12}$, and $Tl_{0.1}In_{0.3}Co_4Sb_{12}$ are shown in Fig. 10.23. A comparison between the κ_{lat} values of $CoSb_3$ and $Tl_{0.1}Co_4Sb_{12}$ reveals a significant reduction of κ_{lat}. This is due to the effective phonon scattering by the rattling of Tl. Moreover, filling with In in addition to Tl yields a further reduction of κ_{lat} in the $Tl_{0.1}In_{0.1}Co_4Sb_{12}$ sample, suggesting that the double-filling approach is effective

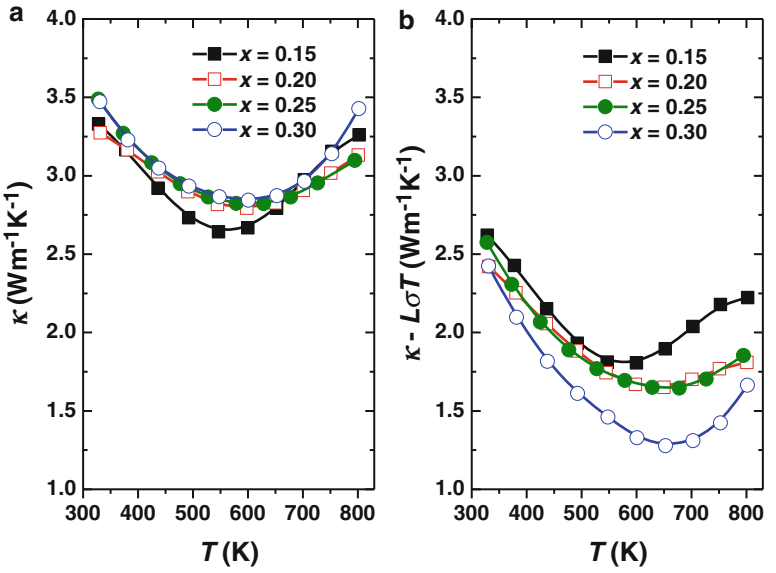

Fig. 10.22 Temperature dependences of the thermal conductivity of polycrystalline samples of $Tl_{0.1}In_xCo_4Sb_{12}$ ($x = 0.15$, 0.20, 0.25, and 0.30); (**a**) total thermal conductivity, κ and (**b**) lattice thermal conductivity, κ_{lat}

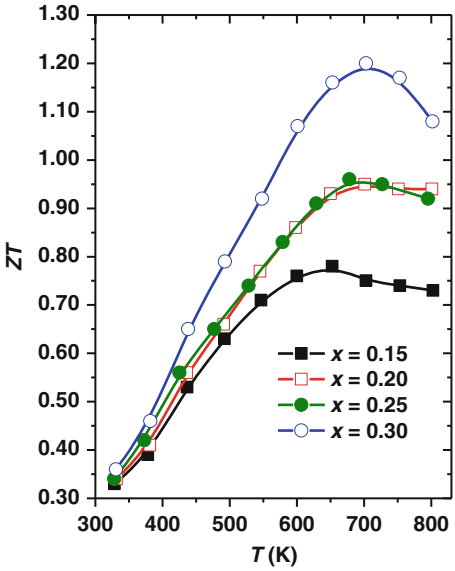

Fig. 10.23 Temperature dependences of the dimensionless figure of merit, ZT of polycrystalline samples of $Tl_{0.1}In_xCo_4Sb_{12}$ ($x = 0.15$, 0.20, 0.25, and 0.30)

for phonon scattering, and hence in reducing κ_{lat}. Furthermore, it can be confirmed that the κ_{lat} of the $Tl_{0.1}In_{0.3}Co_4Sb_{12}$ sample is much lower than those of the other samples. This implies that the rattling of Tl/In, as well as the In_2O_3 nanoparticles formed at the grain boundaries, scatter heat-carrying phonons, leading to the

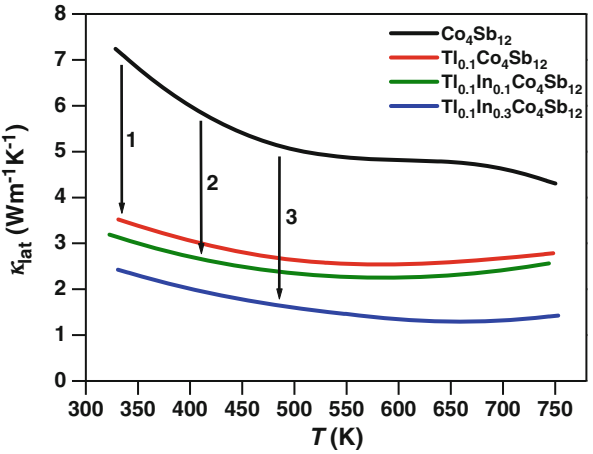

Fig. 10.24 Temperature dependence of the lattice thermal conductivity, κ_{lat} of polycrystalline samples of $CoSb_3$, $Tl_{0.1}Co_4Sb_{12}$, $Tl_{0.1}In_{0.1}Co_4Sb_{12}$, and $Tl_{0.1}In_{0.3}Co_4Sb_{12}$. The numbers *1*, *2*, and *3* in the figure represent phonon scattering by Tl-rattling, Tl- and In-rattling, and Tl- and In-rattling plus In_2O_3 nanoparticles, respectively

dramatic reduction of κ_{lat}. Owing to the very low κ_{lat}, the $Tl_{0.1}In_{0.3}Co_4Sb_{12}$ sample exhibits an excellent *ZT*; its maximum value is 1.20 at around 700 K, as shown in Fig. 10.24.

We can conclude that the Tl/In-double-filled skutterudite exhibits the excellent TE properties. Tl and In are filled up to $x = \sim 0.09$ in $Tl_{0.1}Tl_xCo_4Sb_{12}$ when exceeding the filling limit, In existed as nano-sized In_2O_3 (<50 nm) at grain boundaries. By investigating the TE properties of Tl- and In-double-filled $CoSb_3$-based skutterudites, we demonstrate that the reduction of κ_{lat} is due to the effective phonon scattering induced both by the rattling of Tl and In and by the naturally formed In_2O_3 nanoparticles (<50 nm). This yields a dramatic enhancement of *ZT* to be 1.20 at 700 K. The combined approach of double filling and self-formed nanostructures might be applicable to various clathrate compounds. Thus, these results point to a new strategy in the improvement of bulk TE materials.

10.5 Summary

In this chapter, we reviewed the TE properties of $CoSb_3$-based skutterudites filled by group 13 elements, i.e., the systems of $Tl_xCo_4Sb_{12}$, $Ga_xCo_4Sb_{12}$, and $Tl_{0.1}In_xCo_4Sb_{12}$. The temperature dependence of *ZT* of the best materials in the individual system is summarized in Fig. 10.25.

Tl can be filled in $CoSb_3$ up to around $x = 0.2$ in $Tl_xCo_4Sb_{12}$. Since the valence state of Tl in $CoSb_3$ can be considered to be Tl^{1+}, the Tl-filling yields net increase in electron carriers. Therefore, the carrier concentration of $CoSb_3$ can be controlled by Tl-filling. On the other hand, Tl filled in $CoSb_3$ can act as rattlers and scatter heat carrying phonons efficiently. Therefore, Tl-filled $CoSb_3$ exhibits low κ_{lat} with optimized carrier concentration, and hence high *ZT* value; the maximum *ZT* value is 0.90 at 600 K obtained for $Tl_{0.25}Co_4Sb_{12}$.

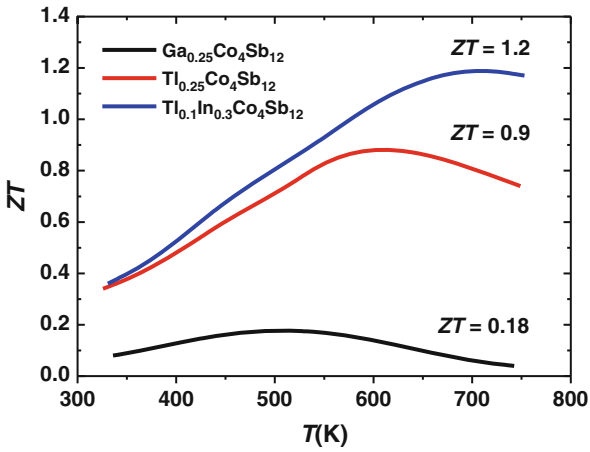

Fig. 10.25 The dimensionless figure of merit, *ZT* of polycrystalline samples of $Tl_{0.25}Co_4Sb_{12}$, $Ga_{0.25}Co_4Sb_{12}$, and $Tl_{0.1}In_{0.3}Co_4Sb_{12}$

In contrast to Tl-filled $CoSb_3$, Ga can be filled in $CoSb_3$ up to only $x = 0.02$ in $Ga_xCo_4Sb_{12}$, and when exceeding the filling limit, Ga exists as metal states mainly at grain boundaries in the polycrystalline samples of $Ga_xCo_4Sb_{12}$. Due to this low filling limit of Ga in $CoSb_3$, carriers are not sufficiently doped by Ga-filling. Nonetheless, not only very small amount of filled Ga but also precipitated Ga metals may scatter heat carrying phonons, leading to the reduction of κ_{lat}. Mainly due to the reduced κ_{lat}, the *ZT* is slightly enhanced by Ga-adding to $CoSb_3$; the maximum *ZT* value is 0.18 at 500 K obtained for $Ga_{0.25}Co_4Sb_{12}$.

In case of the double-filling system, i.e., $Tl_{0.1}In_xCo_4Sb_{12}$, all Tl is filled but In can be filled up to around $x = 0.09$ in $Tl_{0.1}In_xCo_4Sb_{12}$. In added in excess of the filling limit within the samples is in the form of In_2O_3 which is naturally formed as nanoparticles (<50 nm) mainly at the grain boundaries of the polycrystalline samples. Effective phonon scattering occurred both by the rattling of Tl and In and by the naturally formed In_2O_3 nanoparticles yield significant reduction of κ_{lat} and thereby dramatic enhancement of *ZT*. $Tl_{0.1}In_{0.3}Co_4Sb_{12}$ exhibits the maximum *ZT* of 1.20 at around 700 K, which is very high for bulk materials.

We consider the following two studies are important in this research for future. The first one is further enhancement of *ZT* by nanostructuring. Recently, various nanocrystalline bulk materials have been prepared by ball-milling followed by hot-pressing or spark plasma sintering and the enhancement of *ZT* have been achieved [46, 47]. The method is considered to be applied to the $CoSb_3$-based skutterudites. The second one is to develop p-type $CoSb_3$-based skutterudites filled by group 13 elements. Although the $CoSb_3$-based skutterudites filled by group 13 elements reported here have high *ZT* values, all the samples are n-type, i.e., they indicate negative *S* values. However, for a powerful TE module, the similar performances in both n-type and p-type TE materials is required. Therefore, the p-type $CoSb_3$-based skutterudites filled by group 13 elements should be developed. Very recently, our group has demonstrated that $Tl_xFe_yCo_{1-y}Sb_{12}$ exhibit p-type characteristics and relatively high *ZT* values. The details of the results will be reported in near future.

Acknowledgments This work was supported in part by a Grant-in-Aid for Scientific Research (No. 23686091) from the Ministry of Education, Culture, Sports, Science, and Technology, Japan. Additional support was kindly provided by the Rajamangala University of Technology Suvarnabhumi, Thailand, and the Government of Thailand.

References

1. Rowe, D.M.: CRC Handbook of Thermoelectrics. CRC Press, New York (1995)
2. Nolas, G.S., Sharp, J., Goldsmid, H.J.: Thermoelectrics: Basic Principles and New Materials Developments. Springer, New York (2001)
3. Bell, L.E.: Science **321**, 1457 (2008)
4. Ioffe, A.F.: Semiconductor Thermoelements and Thermoelectric Cooling. Infosearch, London (1957)
5. Snyder, G.J., Toberer, E.S.: Nat. Mater. **7**, 105 (2008)
6. Uher, C. In: Tritt, T.M. (ed.) Recent Trends in Thermoelectric Materials Research I, Semiconductors and Semimetals, vol. 69, p. 139. Academic Press, San Diego (2001)
7. Jeitschko, W., Braun, D.: Acta Cryst. **33**, 3401 (1977)
8. Stetson, N.T., Kauzlarich, S.M., Hope, H.: J. Solid State Chem. **91**, 140 (1991)
9. Slack, G.A. In: Rowe, D.M. (ed.) CRC Handbook of Thermoelectrics. CRC Press, New York (1995)
10. Morelli, D.T., Meisner, G.P.: J. Appl. Phys. **77**, 3777 (1995)
11. Sales, B.C., Mandrus, D.G., Chakoumakos, B.C. In: Tritt, T.M. (ed.) Recent Trends in Thermoelectric Materials Research I, Semiconductors and Semimetals, vol. 69. Academic Press, San Diego (2001)
12. Kuznetsov, V.L., Kuznetsova, L.A., Rowe, D.M.: J. Phys. Condens. Matter **15**, 5035 (2003)
13. Nolas, G.S., Cohn, J.L., Slack, G.A.: Phys. Rev. B **58**, 164 (1998)
14. Nolas, G.S., Kaeser, M., Littleton, R.T., Tritt, T.M.: Appl. Phys. Lett. **77**, 1855 (2000)
15. Morelli, D.T., Meisner, G.P., Chen, B.X., Hu, S.Q., Uher, C.: Phys. Rev. B **56**, 7376 (1997)
16. Pei, Y.Z., Bai, S.Q., Zhao, X.Y., Zhang, W., Chen, L.D.: Solid State Sci. **10**, 1422 (2008)
17. Chen, L.D., Kawahara, T., Tang, X.F., Goto, T., Hirai, T., Dyck, J.S., Chen, W., Uher, C.: J. Appl. Phys. **90**, 1864 (2001)
18. Puyet, M., Lenoir, B., Dauscher, A., Dehmas, M., Stiewe, C., Muller, E.: J. Appl. Phys. **95**, 4852 (2004)
19. Zhao, X.Y., Shi, X., Chen, L.D., Zhang, W.Q., Zhang, W.B., Pei, Y.Z.: J. Appl. Phys. **99**, 053711 (2006)
20. Pei, Y.Z., Chen, L.D., Zhang, W., Shi, X., Bai, S.Q., Zhao, X.Y., Mei, Z.G., Li, X.Y.: Appl. Phys. Lett. **89**, 221107 (2006)
21. Pei, Y.Z., Yang, J., Chen, L.D., Zhang, W., Salvador, J.R., Yang, J.H.: Appl. Phys. Lett. **95**, 042101 (2009)
22. Sales, B.C., Chakoumakos, B.C., Mandrus, D.: Phys. Rev. B **61**, 2475 (2000)
23. Nolas, G.S., Takizawa, H., Endo, T., Sellinschegg, H., Johnson, D.C.: Appl. Phys. Lett. **77**, 52 (2000)
24. Nolas, G.S., Yang, J., Takizawa, H.: Appl. Phys. Lett. **84**, 5210 (2004)
25. Fukuoka, H., Yamanaka, S.: Chem. Mater. **22**, 47 (2010)
26. Harnwunggmoung, A., Kurosaki, K., Muta, H., Yamanaka, S.: Appl. Phys. Lett. **96**, 202107 (2010)
27. Keppens, V., Mandrus, D., Sales, B.C., Chakoumakos, B.C., Dai, P., Coldea, R., Maple, M.B., Gajewski, D.A., Freeman, E.J., Bennington, S.: Nature **395**, 876 (1998)
28. Hermann, R.P., Jin, R.J., Schweika, W., Grandjean, F., Mandrus, D., Sales, B.C., Long, G.: Phys. Rev. Lett. **90**, 135505 (2003)

29. Yang, J., Zhang, W., Bai, S.Q., Mei, Z., Chen, L.D.: Appl. Phys. Lett. **90**, 192111 (2007)
30. Shi, X., Kong, H., Li, C.P., Uher, C., Yang, J., Salvador, J.R., Wang, H., Chen, L., Zhang, W.: Appl. Phys. Lett. **92**, 182101 (2008)
31. Bai, S.Q., Pei, Y.Z., Chen, L.D., Zhang, W.Q., Zhao, X.Y., Yang, J.: Acta Mater. **57**, 3135 (2009)
32. Salvador, J.R., Yang, J., Wang, H., Shi, X.: J. Appl. Phys. **107**, 043705 (2010)
33. Zhao, W.Y., Wei, P., Zhang, Q.J., Dong, C.L., Liu, L.S., Tang, X.F.: J. Am. Chem. Soc. **131**, 3713 (2009)
34. Li, H., Tang, X.F., Zhang, Q.J., Uher, C.: Appl. Phys. Lett. **94**, 102114 (2009)
35. Harnwunggmoung, A., Kurosaki, K., Plirdpring, T., Sugahara, T., Ohishi, Y., Muta, H., Yamanaka, S.: J. Appl. Phys. **110**, 013521 (2011)
36. Yang, J., Hao, Q., Wang, H., Lan, Y.C., He, Q.Y., Minnich, A., Wang, D.Z., Harriman, J.A., Varki, V.M., Dresselhaus, M.S., Chen, G., Ren, Z.F.: Phys. Rev. B **80**, 115329 (2009)
37. He, T., Chen, J., Rosenfeld, H.D., Subramanian, M.A.: Chem. Mater. **18**, 759 (2006)
38. Mallik, R.C., Stiewe, C., Karpinski, G., Hassdorf, R., Muller, E.: J. Electron. Mater. **38**, 1337 (2009)
39. Xiong, Z., Chen, X., Huang, X., Bai, S., Chen, L.: Acta Mater. **58**, 3995 (2010)
40. Qiu, Y., Xi, L., Shi, X., Qiu, P., Zhang, W., Chen, L., Salvador, J.R., Cho, J.Y., Yang, J., Chien, Y., Chen, S., Tang, Y., Snyder, G.J.: Adv. Funct. Mater. **23**, 3194 (2013)
41. Li, G., Kurosaki, K., Ohishi, Y., Muta, H., Yamanaka, S.J.: J. Electron. Mater. **42**, 1463 (2013). doi:10.1007/s11664-012-2290-4
42. Caillat, T., Borshchevsky, A., Fleurial, J.-P.: J. Appl. Phys. **80**, 4442 (1996)
43. Harnwunggmoung, A., Kurosaki, K., Kosuga, A., Ishimaru, M., Plirdpring, T., Yimnirun, R., Jutimoosik, J., Rujirawat, S., Ohishi, Y., Muta, H., Yamanaka, S.: J. Appl. Phys. **112**, 043509 (2012)
44. Ballikaya, S., Wang, G., Sun, K., Uher, C.: J. Electron. Mater. **40**, 570 (2011)
45. Deng, L., Jia, X.P., Su, T.C., Zheng, S.Z., Guo, X., Jie, K., Ma, H.A.: Mater. Lett. **65**, 2927 (2011)
46. Poudel, B., Hao, Q., Ma, Y., Lan, Y., Minnich, A., Yu, B., Yan, X., Wang, D., Muto, A., Vashaee, D., Chen, X., Liu, J., Dresselhaus, M.S., Chen, G., Ren, Z.: Science **320**, 634 (2008)
47. Joshi, G., Lee, H., Lan, Y., Wang, X., Zhu, G., Wang, D., Gould, R.W., Cuff, D.C., Tang, M.Y., Dresselhaus, M.S., Chen, G., Ren, Z.: Nano Lett. **8**, 4670 (2008)